Photopatterned Surfaces for Site-Specific and Functional Immobilization of Proteins

José María Alonso,[†] Annett Reichel,[‡] Jacob Piehler,[‡] and Aránzazu del Campo*[,†]

Max-Planck-Institut für Metallforschung, Heisenbergstraβe 3, 70569 Stuttgart, Germany, and Institute of Biochemistry, Johann Wolfgang Goethe-University, 60438 Frankfurt/Main, Germany

Received August 31, 2007. In Final Form: October 8, 2007

Photosensitive silanes containing nitroveratryl (Nvoc)-caged amine groups and protein repellent tetraethylene glycol units were synthesized and used for modification of silica surfaces. Functional surface layers containing different densities of caged amine groups were prepared and activated by UV-irradiation of the surface. The performance of these layers for functional and site-selective immobilization of proteins was tested. For this purpose, biotin and tris-nitrilotriacetic acid (tris-NTA) were fist coupled to the activated surface, and the interaction of streptavidin and His-tagged proteins with the functionalized surfaces was monitored by real-time label-free detection. After optimizing the coupling protocols, highly selective functionalization of the deprotected amine groups was possible. Furthermore, the degree of functionalization (and therefore the amount of immobilized protein) was controlled by diluting the surface concentration of the amine-functionalized silane with a nonreactive (OMe-terminated) tetraethylene glycol silane. Immobilized proteins were highly functional on these surfaces, as demonstrated by protein−protein interaction assays with the type I interferon receptor. Protein micropatterns were successfully generated after masked irradiation and functionalization of the caged surface following the optimized coupling protocols.

Introduction

Miniaturized and high-throughput chemical and biological analysis systems in microarray format have moved to the forefront of the bioanalytical science area. They require only small amounts of analytes and reagents for accurate detection and allow analysis of a variety of samples in parallel.[1] The fabrication of these analytical platforms requires the development of surface patterning strategies able to create a high density of individual and isolated reactive sites on a substrate, onto which the biomolecular species will be immobilized for detection.[2,3] Among them, photoreactive surface layers which can be site-selectively activated upon masked irradiation constitute an interesting patterning alternative with many possible variants. Light can be used (i) to destroy or remove molecular layers at selected positions to render the bare, inactive substrate,[4,5] (ii) to graft molecular species to irradiated regions via photogenerated radical cross-reactions occurring between a photosensitive surface layer and the biological molecule (photoaffinity),[6−10] or (iii) to direct synthesis of small molecules on the surface (peptides,[6,7] oligocarbamates,[8] oligonucleotides,[14−17] and peptoids[9]) through iterative unmasking of photoreactive groups and monomer coupling cycles. Alternatively, surface layers containing the reactive functionalities protected with a photocleavable[19−21] group can be used for site-specific coupling of complementary functionalities after light-deprotection.[6,10−17] The latter is a particularly flexible approach, since a good number of photoremovable groups are known that can be combined with many different reactive species.

Compared to the immobilization of oligonucleotides or peptides, functional immobilization of proteins is much more demanding: surface layers are required for minimizing non-specific interactions of the protein with the surface, which lead to protein denaturation and loss of function of the immobilized protein. Furthermore, functional groups for site-specific tethering of the protein to the surface have to be incorporated. In the case of proteins, surfaces containing oligoethylene glycol (OEG) units within the surface layer are well-known to effectively reduce

* To whom correspondence should be addressed. Telephone: +49 711 6893416. Fax: +49 711 6893412. E-mail: delcampo@mf.mpg.de.

[†] Max-Planck-Institut für Metallforschung.

[‡] Johann Wolfgang Goethe-University.

(1) del Campo, A.; Bruce, I. J. Diagnostics and High Throughput Screening. In *Biomedical Nanotechnology*; Malsch, I., Ed.; CRC Press: Boca Raton, FL, 2005; pp 75−112.

(2) del Campo, A.; Bruce, I. J. *Top. Curr. Chem.* **2005**, *260*, 77−111.

(3) Uttamchandani, M.; Walsh, D. P.; Yao, S. Q.; Chang, Y. T. *Curr. Opin. Chem. Biol.* **2005**, *9* (1), 4−13.

(4) Dulcey, C. S.; Georger, J. H.; Krauthamer, V.; Stenger, D. A.; Fare, T. L.; Calvert, J. M. *Science* **1991**, *252* (5005), 551−554.

(5) Tarlov, M. J.; Burgess, D. R. F.; Gillen, G. *J. Am. Chem. Soc.* **1993**, *115* (12), 5305−5306.

(6) Fodor, S. P. A.; Read, J. L.; Pirrung, M. C.; Stryer, L.; Lu, A. T.; Solas, D. *Science* **1991**, *251* (4995), 767−773.

(7) Pellois, J. P.; Wang, W.; Gao, X. L. *J. Comb. Chem.* **2000**, *2* (4), 355−360.

(8) Cho, C. Y.; Moran, E. J.; Cherry, S. R.; Stephans, J. C.; Fodor, S. P. A.; Adams, C. L.; Sundaram, A.; Jacobs, J. W.; Schultz, P. G. *Science* **1993**, *261* (5126), 1303−1305.

(9) Li, S. W.; Bowerman, D.; Marthandan, N.; Klyza, S.; Luebke, K. J.; Garner, H. R.; Kodadek, T. *J. Am. Chem. Soc.* **2004**, *126* (13), 4088−4089.

(10) Vossmeyer, T.; Jia, S.; DeIonno, E.; Diehl, M. R.; Kim, S. H.; Peng, X.; Alivisatos, A. P.; Heath, J. R. *J. Appl. Phys.* **1998**, *84* (7), 3664−3670.

(11) Sundberg, S. A.; Barrett, R. W.; Pirrung, M.; Lu, A. L.; Kiangsoontra, B.; Holmes, C. P. *J. Am. Chem. Soc.* **1995**, *117* (49), 12050−12057.

(12) del Campo, A.; Boos, D.; Spiess, H. W.; Jonas, U. *Angew. Chem., Int. Ed.* **2005**, *44* (30), 4707−4712.

(13) Jonas, U.; del Campo, A.; Kruger, C.; Glasser, G.; Boos, D. *Proc. Natl. Acad. Sci. U.S.A.* **2002**, *99* (8), 5034−5039.

(14) Yan, F. N.; Chen, L. H.; Tang, Q. L.; Rong, W. *Bioconjugate Chem.* **2004**, *15* (5), 1030−1036.

(15) Ryan, D.; Parviz, B. A.; Linder, V.; Semetey, V.; Sia, S. K.; Su, J.; Mrksich, M.; Whitesides, G. M. *Langmuir* **2004**, *20* (21), 9080−9088.

(16) Dendane, N.; Hoang, A.; Guillard, L.; Defrancq, E.; Vinet, F.; Dumy, P. *Bioconjugate Chem.* **2007**, *18* (3), 671−676.

(17) Critchley, K.; Jeyadevan, J. P.; Fukushima, H.; Ishida, M.; Shimoda, T.; Bushby, R. J.; Evans, S. D. *Langmuir* **2005**, *21* (10), 4554−4561.

(18) Oklejas, V.; Harris, J. M. *Langmuir* **2003**, *19* (14), 5794−5801.

(19) Folkers, J. P.; Laibinis, P. E.; Whitesides, G. M. *Langmuir* **1992**, *8* (5), 1330−1341.

(20) Tamada, K.; Hara, M.; Sasabe, H.; Knoll, W. *Langmuir* **1997**, *13* (6), 1558−1566.

(21) Fadeev, A. Y.; McCarthy, T. J. *Langmuir* **1999**, *15* (21), 7238−7243.

10.1021/la702696b CCC: $40.75
Published on Web 12/20/2007

nonspecific interactions.[30,31] Accordingly, different strategies have been followed to incorporate OEG units to a functional surface: direct coupling of surface active functionality through OEG linkers, coadsorption from a solution of OEG and functional molecules (in either parallel[18−20] or sequential[21] surface reactions), or the use of branched surface coupling agents containing protein repellent and protein attractive arms.[36−40] From these three possibilities, competitive chemisorption by treating the surface with a mixture of reagents allows controlled dilution of surface functionality to adjust the surface properties precisely.

Here, we have synthesized novel photosensitive silanes designed for patterned and functional protein immobilization, namely, a tetraethylene glycol (TEG) triethoxysilane with a terminal amino group protected by the nitroveratryl (Nvoc) group, and a methoxy-terminated TEG triethoxysilane. The properties of monocomponent and mixed surface layers obtained from these silanes were characterized in detail. The performance of these surfaces for a site-specific and functional immobilization of proteins was explored by real-time label-free detection. We demonstrate the capability of these surfaces to generate laterally resolved functional protein patterns.

Experimental Section

Materials. All reagents were, unless otherwise noted, used as purchased. Tetrahydrofuran (THF) and toluene were freshly distilled from sodium benzophenone. All reactions were performed under an atmosphere of dry nitrogen. Analytical thin-layer chromatography (TLC) was performed with silica gel 60 F_{254} plates. Visualization was accomplished by UV light and $KMnO_4$ solution. Silicon wafers (100 orientation) were provided by Crystec (Berlin, Germany). Quartz substrates (Suprasil) were purchased from Heraeus Quarzglas (Hanau, Germany) and Quarzschmelze Ilmenau (Langewiesen, Germany). Transducer slides for reflectance interference spectroscopy (10 nm Ta_2O_5 and 325 nm silica on a glass substrate) were obtained from Analytik Jena GmbH, Germany. OtBu-protected tris-nitrilotriacetic acid (tris-NTA)-functionalized with a carboxyl group **(9)** and ^{BT}tris-NTA were synthesized as published previously.[22−25] The proteins MBP-H10, ifnar2-H10, and IFNα2 were expressed in *E. coli* and purified as published previously.[24,26]

^{1}H NMR (250 MHz) and ^{13}C NMR (65 MHz) spectra were recorded in $CDCl_3$ using chloroform as an internal reference with a Bruker Ultra Shield 250 MHz spectrometer (Bruker BioSpin GmbH, Rheinstetten, Germany). Chemical shifts (δ) are given in ppm; multiplicities are indicated by s (singlet), d (doublet), dd (double-doublet), ddt (double-double-triplet), q (quadruplet), or m (multiplet). Coupling constants (J) are reported in Hertz. Mass spectra (MS) were obtained at 70 eV by chemical ionization (CI) in a Clarus 500 GCMS spectrometer (Perkin-Elmer, Waltham, MA). Data are reported in the form m/z (intensity relative to base = 100).

Synthesis. *Tetraethylene Glycol Monoallyl Ether (**1**).*[27] Tetraethylene glycol (10 g, 51 mmol), an equimolar amount of allyl chloride (3.9 g, 51 mmol), and tetrabutyl ammonium hydrogen sulfate (1.1 g, 3 mmol) were dissolved in dichloromethane. A 50% aqueous solution of NaOH (40 mL, 0.5 mol) was added slowly under vigorous stirring. The reaction was allowed to proceed for other 20 h at room temperature. The organic layer was separated, and the aqueous layer was washed three times with dichloromethane. The organic fractions were collected, dried over sodium sulfate, and filtered. After evaporation of the solvent, the residue was purified by column chromatography on silica, using ethyl acetate/ethanol 9/1 as eluent to give compound **1** (4.1 g, 31%) as a colorless oil. Disubstituted product was also obtained in 14% yield. ^{1}H NMR ($CDCl_3$) δ 3.48−3.61 (m, 17H), 3.91 (dd, $^3J_{HH}$ = 5.7 Hz, $^2J_{HHgem}$ = 1.3 Hz, 2H), 5.06 (dd, $^3J_{HHcis}$ = 10.4 Hz, $^2J_{HHgem}$ = 1.6 Hz, 1H), 5.16 (dd, $^3J_{HHtrans}$ = 18.0 Hz, $^2J_{HHgem}$ = 1.6 Hz, 1H), 5.80 (ddt, $^3J_{HHtrans}$ = 17.1 Hz, $^3J_{HHcis}$ = 10.4 Hz, $^3J_{HH}$ = 5.6 Hz, 1H) ppm. ^{13}C NMR ($CDCl_3$) δ 61.1, 69.1, 70.0, 70. 3, 71.8, 72.4, 116.6, 134.6 ppm. MS (CI) m/z 234 (M^+ + 1, 100).

*Tetraethylene Glycol Monoallyl Ether Bromide (**2**).*[28] To a solution of **1** (5 g, 21 mmol) in dry THF (85 mL), CBr_4 (10.5 g, 31.5 mmol) and PPh_3 (8.3 g, 31.5 mmol) were added slowly at 0 °C. The mixture was stirred at room temperature for 16 h and filtered. THF was then removed under vacuum, and the residue was purified by silica column chromatography eluting ethyl acetate/hexane 1.5/1 to yield compound **2** (5.3 g, 85%) as a pale yellow oil. ^{1}H NMR ($CDCl_3$) δ 3.46 (t, $^3J_{HH}$ = 6.4 Hz, 2H), 3.57−3.70 (m, 12H), 3.80 (t, $^3J_{HH}$ = 6.3 Hz, 2H), 4.01 (d, $^3J_{HH}$ = 5.7 Hz, 2H), 5.17 (dd, $^3J_{HHcis}$ = 10.4 Hz, $^2J_{HHgem}$ = 1.7 Hz, 1H), 5.26 (dd, $^3J_{HHtrans}$ = 17.2 Hz, $^2J_{HHgem}$ = 1.7 Hz, 1H), 5.91 (ddt, $^3J_{HHtrans}$ = 17.2 Hz, $^3J_{HHcis}$ = 10.3 Hz, $^3J_{HH}$ = 5.6 Hz, 1H) ppm. ^{13}C NMR ($CDCl_3$) δ 30.2, 69.4, 70.5, 70.6, 71.2, 72.2, 117.1, 134.8 ppm. MS (CI) m/z 299 (M^+ + 1, 2), 151 ($M^+ - C_7H_{13}O_3$, 25).

*Tetraethylene Glycol Monoallyl Ether Phthalimide (**3**).*[28] A dimethylformamide (DMF) solution (50 mL) containing compound **2** (2 g, 6.7 mmol), phthalimide (2 g, 13.4 mmol), and potassium carbonate (0.94 g, 6.7 mmol) was heated at 85 °C for 18 h. The mixture was filtered, and the solvent was removed under vacuum. The oily residue was subjected to column chromatography on silica, eluting with ethyl acetate/hexane 1/1 to afford compound **3** (1.7 g, 69%) as a colorless oil. ^{1}H NMR ($CDCl_3$) δ 3.55−3.68 (m, 12H), 3.71 (t, $^3J_{HH}$ = 5.7 Hz, 2H), 3.87 (t, $^3J_{HH}$ = 6.4 Hz, 2H), 3.99 (d, $^3J_{HH}$ = 5.7 Hz, 2H), 5.14 (dd, $^3J_{HHcis}$ = 10.3 Hz, $^2J_{HHgem}$ = 1.7 Hz, 1H), 5.24 (dd, $^3J_{HHtrans}$ = 17.2 Hz, $^2J_{HHgem}$ = 1.7 Hz, 1H), 5.88 (ddt, $^3J_{HHtrans}$ = 17.2 Hz, $^3J_{HHcis}$ = 10.3 Hz, $^3J_{HH}$ = 5.6 Hz, 1H) ppm. ^{13}C NMR ($CDCl_3$) δ 37.0, 67.5, 69.1, 69.8, 70.2, 71.7, 116.3, 122.8, 131.7, 133.7, 134.7 ppm. MS (CI) m/z 174 ($M^+ - C_{10}H_7NO_3$, 100), 218 ($M^+ - C_8H_3NO_2$, 5).

*Tetraethylene Glycol Monoallyl Ether Amine (**4**).*[28] To a solution of compound **3** (2 g, 5.5 mmol) in ethanol, hydrazine monohydrate (0.56 g, 11 mmol) was added. The mixture was heated at reflux for 6 h and allowed to warm to room temperature. The white precipitate was removed by filtration, and the solvent was removed under vacuum. The residue was then diluted with water and extracted three times with dichloromethane. The combined organic layers were dried over anhydrous sodium sulfate and evaporated under vacuum to give compound **4** (1.0 g, 79%) as a colorless oil. ^{1}H NMR ($CDCl_3$) δ 1.71 (s, 2H), 2.85 (t, $^3J_{HH}$ = 5.2 Hz, 2H), 3.50 (t, $^3J_{HH}$ = 5.2 Hz, 2H), 3.59−3.68 (m, 12H), 4.01 (d, $^3J_{HH}$ = 5.7 Hz, 2H), 5.17 (dd, $^3J_{HHcis}$ = 10.4 Hz, $^2J_{HHgem}$ = 1.4 Hz, 1H), 5.26 (dd, $^3J_{HHtrans}$ = 17.2 Hz, $^2J_{HHgem}$ = 1.6 Hz, 1H), 5.90 (ddt, $^3J_{HHtrans}$ = 17.2 Hz, $^3J_{HHcis}$ = 10.4 Hz, $^3J_{HH}$ = 5.6 Hz, 1H) ppm. ^{13}C NMR ($CDCl_3$) δ

(22) Lata, S.; Gavutis, M.; Tampe, R.; Piehler, J. *J. Am. Chem. Soc.* **2006**, *128* (7), 2365−2372.
(23) Lata, S.; Reichel, A.; Brock, R.; Tampe, R.; Piehler, J. *J. Am. Chem. Soc.* **2005**, *127* (29), 10205−10215.
(24) Lata, S.; Piehler, J. *Anal. Chem.* **2005**, *77* (4), 1096−1105.
(25) Reichel, A.; Schaible, D.; Al Furoukh, N.; Cohen, M.; Schreiber, G.; Piehler, J. *Anal. Chem.* **2007**, *79* (22), 8590−8600.
(26) Piehler, J.; Schreiber, G. *J. Mol. Biol.* **1999**, *289* (1), 57−67.
(27) Delamarche, E.; Donzel, C.; Kamounah, F. S.; Wolf, H.; Geissler, M.; Stutz, R.; Schmidt-Winkel, P.; Michel, B.; Mathieu, H. J.; Schaumburg, K. *Langmuir* **2003**, *19*, 8749−8758.
(28) Jeong, K. S.; Park, E. J. *J. Org. Chem.* **2004**, *69*, 2618−2621.
(29) Effenberger, F.; Heid, S. *Synthesis* **1995**, 1126−1130.
(30) Brecht, A.; Gauglitz, G. *Biosens. Bioelectron.* **1995**, *10* (9−10), 923−36.
(31) Hanel, C.; Gauglitz, G. *Anal. Bioanal. Chem.* **2002**, *372* (1), 91−100.
(32) Schmitt, H. M.; Brecht, A.; Piehler, J.; Gauglitz, G. *Biosens. Bioelectron.* **1997**, *12* (8), 809−816.
(33) Bunker, B. C.; Carpick, R. W.; Assink, R. A.; Thomas, M. L.; Hankins, M. G.; Voigt, J. A.; Sipola, D.; de Boer, M. P.; Gulley, G. L. *Langmuir* **2000**, *16* (20), 7742−7751.
(34) Kallury, K. M. R.; Macdonald, P. M.; Thompson, M. *Langmuir* **1994**, *10* (2), 492−499.
(35) Bierbaum, K.; Kinzler, M.; Woll, C.; Grunze, M.; Hahner, G.; Heid, S.; Effenberger, F. *Langmuir* **1995**, *11* (2), 512−518.
(36) Britcher, L. G.; Kehoe, D. C.; Matisons, J. G.; Smart, R. S. C.; Swincer, A. G. *Langmuir* **1993**, *9* (7), 1609−1613.
(37) Fadeev, A. Y.; McCarthy, T. J. *Langmuir* **2000**, *16* (18), 7268−7274.
(38) Piehler, J.; Brecht, A.; Hehl, K.; Gauglitz, G. *Colloids Surf., B* **1999**, *13* (6), 325−336.
(39) Piehler, J.; Brecht, A.; Valiokas, R.; Liedberg, B.; Gauglitz, G. *Biosens. Bioelectron.* **2000**, *15* (9−10), 473−481.
(40) Maisch, S.; Buckel, F.; Effenberger, F. *J. Am. Chem. Soc.* **2005**, *127*, 17315−17322.

40.1, 69.3, 69.6, 70.0, 70.1, 70.4, 72.6, 117.0, 134.6 ppm. MS (CI) *m*/*z* 234 ($M^+ + 1$, 100).

*N-Nvoc Tetraethylene Glycol Monoallyl Ether Carbamate (**5**).*[12] Compound **4** (1 g, 4.3 mmol), sodium hydrogencarbonate (0.84 g, 10.8 mmol), and water were placed into a dry round-bottom flask and cooled in an ice bath. Nvoc-Cl (1.2 g, 4.3 mmol) was dissolved in dioxane (40 mL) and added dropwise under vigorous stirring. The mixture was allowed to stir at room temperature overnight and then was extracted three times with dichloromethane. The organic layers were dried over sodium sulfate and evaporated under vacuum. The solid residue was purified by silica column chromatography eluting ethyl acetate/ethanol 98/2 to afford compound **5** (1.6 g, 79%) as a pale yellow oil. ^{1}H NMR ($CDCl_3$) δ 3.41 (q, $^3J_{HH} = 5.2$ Hz, 2H), 3.58 (t, $^3J_{HH} = 5.1$ Hz), 3.63−3.71 (m, 12H), 3.95 (s, 3H), 3.98 (s, 3H), 4.00−4.03 (m, 2H), 5.16 (dd, $^3J_{HHcis} = 10.3$ Hz, $^2J_{HHgem} = 1.4$ Hz, 1H), 5.25 (dd, $^3J_{HHtrans} = 17.2$ Hz, $^2J_{HHgem} = 1.6$ Hz, 1H), 5.51 (s, 3H), 5.81−5.97 (m, 1H), 7.02 (s, 1H), 7.70 (s, 1H) ppm. ^{13}C NMR ($CDCl_3$) δ 40.9, 56.3, 63.3, 69.3, 69.9, 70.2, 70.5, 72.1, 108.1, 110.0, 117.0, 128.4, 134.7, 139.7, 148.0, 153.5, 155.9 ppm. MS (CI) *m*/*z* 196 ($M^+ - C_{12}H_{22}NO_6$, 100), 203 ($M^+ - C_{11}H_{13}N_2O_6$, 10).

*N-Nvoc Tetraethylene Glycol Monoallyl Ether Carbamate (3-Triethoxysilyl)propyl Ether (**6**).*[29] Compound **5** (1 g, 2.1 mmol) and triethoxysilane (3.4 g, 21 mmol) were placed in a previously passivated dry round-bottom flask and heated under Ar atmosphere to about 85 °C. At this temperature, both reactants mix homogeneously. A solution of $H_2PtCl_6 \cdot H_2O$ in *i*-PrOH (0.10 mL, 65 mM) was then dropped, and the mixture was stirred for 5 h at 85 °C and then allowed to cool down. An excess of triethoxysilane was removed in vacuum, and the residue was purified by chromatography performed with passivated silica gel (see "Purification of the Derivatized Triethoxysilanes by Passivated Silica Gel Chromatography" in the Experimental section) using ethyl acetate/ethanol 97/3 as eluent to afford compound **6** (0.70 g, 52%) as a pale orange oil. The saturated byproduct (<20%) was also obtained. ^{1}H NMR ($CDCl_3$) δ 0.60 (t, $^3J_{HH} = 8.5$ Hz, 2H), 1.25 (t, $^3J_{HH} = 7.0$ Hz, 9H), 1.61−1.73 (m, 2H), 3.30−3.43 (m, 4H), 3.55−3.68 (m, 14H), 3.82 (q, $^3J_{HH} = 7.0$ Hz, 6H), 3.94 (s, 3H), 3.97 (s, 3H), 5.51 (s, 2H), 5.67 (s, 1H), 7.03 (s, 1H), 7.70 (s, 1H) ppm. ^{13}C NMR ($CDCl_3$) δ 6.4, 18.3, 22.9, 41.0, 63.4, 70.0, 70.6, 73.6, 108.1, 110.1, 128.4, 140.0, 148.0, 153.5, 156.0 ppm. MS (CI) *m*/*z* 378 ($M^+ - C_{10}H_{14}N_2O_6$, 100), 441 ($M^+ - C_9H_9NO_4$, 52).

*Tetraethylene Glycol Allyl Methyl Ether (**7**).*[27] Tetraethylene glycol monomethyl ether (10 g, 47 mmol), an equimolar amount of allyl chloride (3.6 g, 47 mmol), and tetrabutyl ammonium hydrogen carbonate (1.0 g, 2.8 mmol) were dissolved in dichloromethane. A 50% aqueous solution of NaOH (36 mL, 0.36 mol) was added slowly under vigorous stirring. The reaction was allowed to proceed for another 20 h at room temperature. The organic layer was then separated, washed three times with water, dried over sodium sulfate, and filtered. After evaporation of the solvent, the residue was purified by column chromatography on silica using ethyl acetate/ethanol 9/1 as eluent to give compound **7** (6.5 g, 56%) as a colorless oil. ^{1}H NMR ($CDCl_3$) δ 3.20 (s, 3H), 3.42−3.47 (m, 17H), 3.83 (dd, $^3J_{HH} = 5.6$ Hz, $^2J_{HHgem} = 1.2$ Hz, 2H), 5.03 (dd, $^3J_{HHtrans} = 17.2$ Hz, $^2J_{HHgem} = 1.6$ Hz, 1H), 5.80 (m, 1H) ppm. ^{13}C NMR ($CDCl_3$) δ 58.8, 69.3, 70.1, 70.3, 70.4, 71.8, 72.0, 72.3, 116.7, 134.7 ppm. MS (CI) *m*/*z* 103 ($M^+ - C_7H_{13}O_3$, 100).

*Tetraethylene Glycol Methyl Ether (3-Triethoxysilyl)propyl Ether (**8**).*[29] Tetraethylene glycol allyl methyl ether **7** (3.0 g, 12.1 mmol) and triethoxysilane (23.4 g, 121 mmol) were placed in a previously passivated dry round-bottom flask and heated under Ar atmosphere to about 85 °C. At this temperature, both reactants mix homogeneously. A solution of $H_2PtCl_6 \cdot H_2O$ in *i*-PrOH (0.54 mL, 65 mM) was then dropped, and the mixture was stirred for 5 h at 85 °C and then allowed to cool down. An excess of triethoxysilane was removed in vacuum, and the residue was purified by chromatography performed with passivated silica gel (see "Purification of the Derivatized Triethoxysilanes by Passivated Silica Gel Chromatography" in the Experimental section) using ethyl acetate/hexane/ethanol 85/15/5 as eluent to afford compound **8** (1.8 g, 35%) as a pale yellow oil. A small proportion of saturated byproduct (<10%) was also obtained. ^{1}H NMR ($CDCl_3$) δ 0.58−0.65 (m, 2H), 1.21 (t, $^3J_{HH} = 7.0$ Hz, 9H), 1.65−1.92 (m, 2H), 3.37−3.45 (m, 5H), 3.52−3.65 (m, 16H), 3.80 (q, $^3J_{HH} = 7.0$ Hz, 6H) ppm. ^{13}C NMR ($CDCl_3$) δ 6.3, 18.0, 22.8, 58.2, 59.0, 69.8, 69.9, 70.3, 70.4, 70.5, 71.2, 73.4 ppm. MS (CI) *m*/*z* 430 ($M^+ + 18$, 100).

Purification of the Derivatized Triethoxysilanes by Passivated Silica Gel Chromatography. The silica gel needed for column chromatography was stirred for 10 min in a 2% solution of hexamethyldisilazane (HMDS) in the corresponding eluent. A change in the sedimentation properties of the slurry provides experimental evidence of the changes that occur on the surface chemistry of the particles during passivation (the particles sediment quicker by no stirring once they have been passivated with HMDS). After filling the column with this mixture, immediate washing with the eluent is necessary to get rid of the excess HMDS. Following this procedure, only a slight decrease in the polarity of the silica was noticed and this could be easily counteracted by a slight lowering of the polarity of the eluent mixture (as an example, when the elected eluent was ethylacetate/ethanol 97/3 according to the thin layer chromatography experiments, the eluent ratio for the real separation was 98/2). After washing, the chromatographic separation process was performed as usual.

Silanization. Quarz slides (25 mm × 10 mm × 1 mm) and silicon wafers (25 mm × 10 mm × 1 mm) were cleaned by soaking in freshly prepared Piranha solution (H_2SO_4/H_2O_2 5/1) for one night, rinsing with deionized water, and drying in vacuum at 90 °C for 1 h. Glassware was passivated prior to surface reaction by exposure in HMDS atmosphere at room temperature and in vacuum overnight. This step avoids undesired reactant consumption during surface silanisation due to the condensation of the triethoxysilane groups with the free Si−OH groups at the surface of the glass reactors. The surface modification process was performed following a published protocol.[12,13] Experiments with increasing catalyst concentration and deposition times were performed to obtain smooth and homogeneous layers with a maximum density of functional groups (as revealed by UV spectroscopy). In an optimized procedure, a 1% solution of the corresponding silane in THF with traces of NaOH (40 μL of 1 N aq NaOH in 17 mL of THF) was prehydrolyzed for 4 h and filtered (0.2 μm PTFE filter) before the clean substrates were immersed for 24 h. Afterward, the substrates were washed with THF and Milli-Q water, baked at 90 °C in vacuum for 1 h, sonicated in THF (three times for 2 min each), washed with Milli-Q water, and then dried with a N_2 stream. Mixed layers were obtained by immersing the substrates in a 1% solution of selected silane mixtures (1:1, 1:2, 1:4, 1:9) following the same protocol as that for monocomponent layers.

Photo-deprotection. Activation of the surface functionality by photocleavage of the Nvoc group was achieved by irradiation of the substrates at 365 nm, carried out using a Polychrome V monochromator coupled to a Xe-lamp (1.2 mW cm^{-2} at 365 nm) (TILL Photonics GmbH, Gräfelfing, Germany). The substrates were washed with THF after irradiation to remove the photolysis side products from the surface. The deprotection was monitored by the decay in the UV−vis spectrum (as a consequence of the cleavage of the chromophore). The minimum irradiation time for full deprotection was obtained from different experiments at various irradiation times. For laterally structured deprotection, quartz slides with chrome patterned fields containing micrometric stripes (from ML&C, Jena, Germany) were placed on top of the substrate during irradiation.

Surface Characterization. UV spectra of quartz substrates silanized with **6** and **8** were recorded on a Varian Cary 4000 UV−vis spectrometer (Varian Inc. Palo Alto, CA). Static water contact angles of modified silicon wafers were measured on a OCA 30 Contact Angle system (SCA 202 Software) from DataPhysics Instruments GmbH (Filderstadt, Germany). The equipment was combined with a charge-coupled device (CCD) camera for image capturing. Layer thickness was measured on modified silicon wafers using a ELX-02C ellipsometer by DRE-Dr. Riss Ellipsometerbau GmbH (Ratzeburg, Germany). The refractive index was assumed to be 1.4571 in the deposited layers in a three phase model (silicon substrate/silica + organic layer/air). The thickness of the native silica layer was measured before silanization and was found to be between 1.9 and 2.1 nm.

Scheme 1. (a) Synthetic Route to Silanes 6 and 8. (b) Surface Functionalization with Tris-NTA

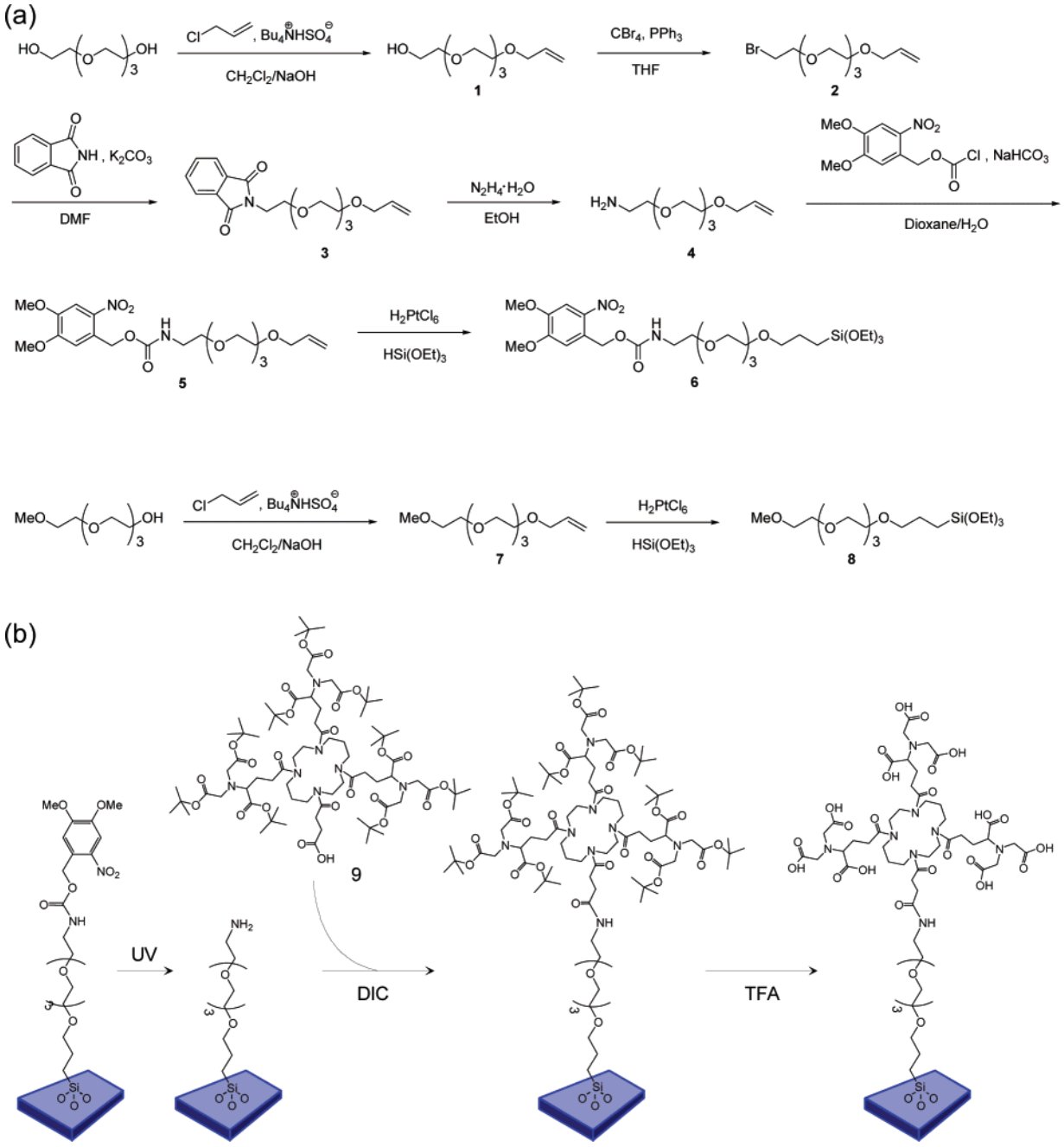

Surface Functionalization for Protein Studies. Prior to activation of the surface functionality by photocleavage of the Nvoc group, the substrates modified with **6**, **8**, or mixtures of both were incubated in acetic anhydride at room temperature for 15 min and then thoroughly rinsed with THF and water and dried with nitrogen. For functionalization with tris-NTA, 5 μL of a solution of **9** in chloroform (100 mg mL^{-1}) was homogeneously applied onto the surface and the solvent was evaporated in a nitrogen stream. The coupling reaction was initiated by addition of 5 μL of DIC, which was subsequently incubated for 10−30 min at room temperature by assembling the surfaces of two slides face to face. The excess reaction mixture was washed off with chloroform, acetone, and then water. The substrates were then incubated in trifluoroacetic acid (TFA) overnight to cleave the *tert*-butyl esters and liberate the NTA chelator heads.

For biotin-functionalized surfaces, 5 μL of *N*-(+)-biotinyl-6-aminocaproic acid-*N*-hydroxysuccinimidyl ester in DMF (50 mg mL^{-1}) was homogeneously applied onto the surface, after blocking with acetic anhydride. The transducers were incubated for 15 min at room temperature by assembling the surfaces of two slides face to face. The excess reaction mixture was washed off with DMF and water. The transducers were then dried with nitrogen and stored at −20 °C.

Protein Binding Experiments. Protein immobilization and protein interactions were label-free monitored in real time using reflectance interference spectroscopy (RIFS). This technique detects binding on the surface of a thin silica layer as a shift of the interference spectrum,[30] which was determined at the minimum 1.5th order. A shift of this minimum by 1 nm corresponds to a change in the optical thickness of the interference layer by 0.75 nm and to a surface mass change of ~1 ng/mm^2.[31] A home-built setup based on a commercially available diode array spectrometer as described before was used.[32] Measurements were carried out in a flow chamber under continuous flow with a data acquisition rate of 1 Hz. All binding assays were carried out with HBS (20 mM Hepes, pH 7.5, 150 mM NaCl, 0.01% Triton X100) as the running buffer. The tris-NTA-functionalized surfaces were treated with 100 mM HCl for 150 s, followed by equilibration in HBS. The chelator heads were loaded with nickel(II) ions by injecting 250 μL of nickel(II) chloride (10 mM) for 30

Table 1. Static Water Contact Angles (CA), Ellipsometric Layer Thickness (*d*), and Surface Loading (Γ) as Estimated from *d* of the Mono- and Bicomponent Surface Layers Obtained before and after Irradiation

molar ratio of silane **6**:**8** in solution	before irradiation							after irradiation	
	CA	*d* (nm)[a]	ρ (g cm^{-3})[b]	Γ (ng mm^{-2})[c]	Γ (pmol mm^{-2})[c]	Γ (molecs mm^{-2})[c]	Γ_{NH2} (pmol mm^{-2})[d]	CA	*d* (nm)
1:0	57° ± 2	2.65 ± 0.11	1.113	2.95	5.51	3.2×10^{12}	5.51	49° ± 2	1.98 ± 0.41
1:1	52° ± 2	2.00 ± 0.95	1.113	2.26	5.53	3.3×10^{12}	2.06	47° ± 2	1.67 ± 0.17
1:4	51° ± 2	1.63 ± 0.15	1.113	1.81	5.11	3.1×10^{12}	0.67	49° ± 2	1.37 ± 0.20
1:9	55° ± 2	1.46 ± 0.13	1.113	1.62	4.78	2.9×10^{12}	0.29	52° ± 1	1.31 ± 0.06
0:1	51° ± 2	1.05 ± 0.11	1.113	1.17	3.6	2.1×10^{12}	0		

[a] *d* = Ellipsometric layer thickness. [b] ρ = Layer density estimated assuming ρ = 1.0 g cm^{-3} for *n* = 1.43 and $\Delta n/\Delta\rho = 0.24$. [c] Γ = Surface loading calculated from ρ and *d*. [d] Γ_{NH2} = Surface loading of amine groups calculated assuming equivalent molar fractions of silane **6** on the surface and in solution.

s, followed by injection of 500 μL of histidine (His)-tagged protein (500 nM) for 400 s. The elution of the immobilized protein with 200 mM imidazole was then monitored for 140 s. The surface was regenerated via injection of 250 μL of HCl (100 mM) for 30 s, followed by the nickel loading step. Biotin-functionalized surfaces were first loaded with streptavidin by injecting 250 μL of streptavidin (100 nM) for 150 s. For immobilizing His-tagged proteins on top of the streptavidin layer, 350 nM ^{BT}tris-NTA was injected for 30 s, followed by injection of 500 μL of MBP-H10 (500 nM) for 400 s. The activity of the immobilized ifnar2-H10 was probed by monitoring the binding of its ligand IFNα2 upon injection of 300 μL of IFNα2 (100 nM) for 30 s. The proteins were eluted by injecting 400 mM imidazole for 140 s. Negative control experiments were performed in the absence of nickel(II) ions. To demonstrate the specificity of the binding event, the NTA-bound nickel(II) ions were removed by an injection of 250 μL of ethylenediaminetetraacetic acid (EDTA) (250 mM) before injection of the protein.

Functional Properties of Patterned Surfaces. Patterned substrates modified with **6** were masked irradiated and then incubated with a 140 μg mL^{-1} solution of Alexa Fluor 546 succinimidyl ester in dimethyl sulfoxide (DMSO) at room temperature overnight. The substrate was then washed with water and THF and dried with a N_2 stream. The fluorescent pattern was visualized by fluorescence imaging with an Axio Imager Z1 instrument (Software Axio Vision Rel. 4.6) from Carl Zeiss GmbH (Göttingen, Germany). Biotinylated surfaces were incubated with 1.5 μM streptavidin in buffer (PBS, 0.01% Triton X100) for 2 h. The substrate was washed with buffer (PBS, 0.01% Triton X100), dried in a stream of nitrogen, and incubated with 100 μL of a solution of 230 μM biotin-4-fluorescein in buffer (PBS, 0.01% Triton X100) for 75 min. Finally, the substrate was washed with PBS buffer and water, dried in a stream of nitrogen, and preserved from the light until analysis by fluorescence microscopy.

Results and Discussion

Synthesis of the TEG Silanes. Two triethoxysilanes, one carrying a photocleavable nitroveratryloxycarbonyl (−Nvoc) protected amine (**6**) and another with an inert methoxy (**8**) headgroup functionality, were synthesized (Scheme 1). A protein repellent tetraethyleneglycol chain separates the headgroup and the triethoxysilane anchor group in the molecules. The synthetic route followed to obtain the photoactive silane **6** starts with a desymmetrization reaction to obtain the unsaturated TEG derivative **1**. The free OH functionality was then transformed into a free amino group by bromation (**2**), followed by reaction with phthalimide (Gabriel synthesis) and deprotection using hydrazine to obtain **4**. Reaction of the amine with nitroveratryl chloroformate under Schotten−Baumann conditions yielded the caged derivative as carbamate (**5**) in good yields. Hydrosilylation of the double bond is performed as the last step to prevent unwanted hydrolysis and condensation reactions of the labile triethoxysilane functionality. Hydrosilylation was performed with triethoxysilane and H_2PtCl_6 as catalyst and afforded the expected photosensitive triethoxysilane **6** with high yield. A 15−30% fraction of saturated side product is present in the reaction mixture after evaporation of the excess of triethoxysilane. Similar reaction steps were followed for obtaining the molecule **8**.

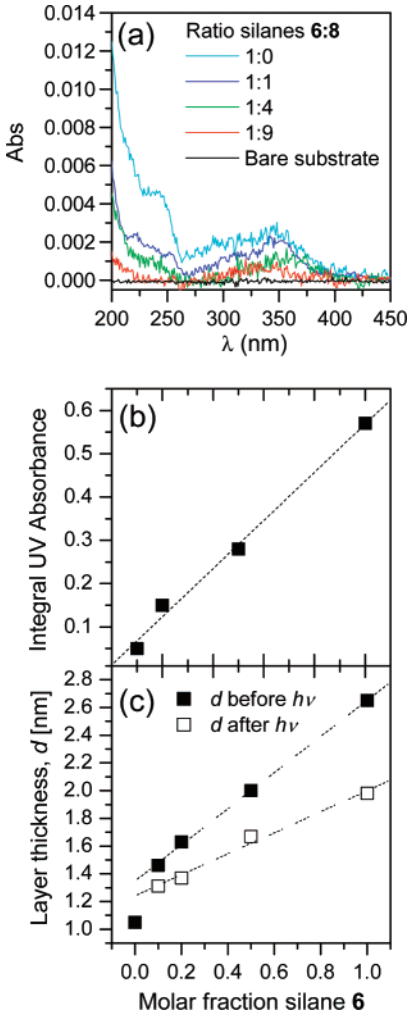

Figure 1. (a) UV spectra of quartz substrates modified with feeding solutions with different concentrations of silanes **6** and **8.** (b) Integral of the UV spectra showing the linear relationship between the molar fraction of silane **6** in solution and the UV absorbance at the surface. (c) Variation of the layer thickness with solution composition for the different mixtures.

Since high purity reactants are required for reproducible surface modification experiments, especially if contaminants carry alkoxysilane functions, a careful purification process must be performed. Purification by chromatography with silica gel led to low yields of purified substance (<10%) as a consequence of the condensation reaction of the alkoxysilane groups of the molecule with the Si−OH groups at the surface of the silica gel.

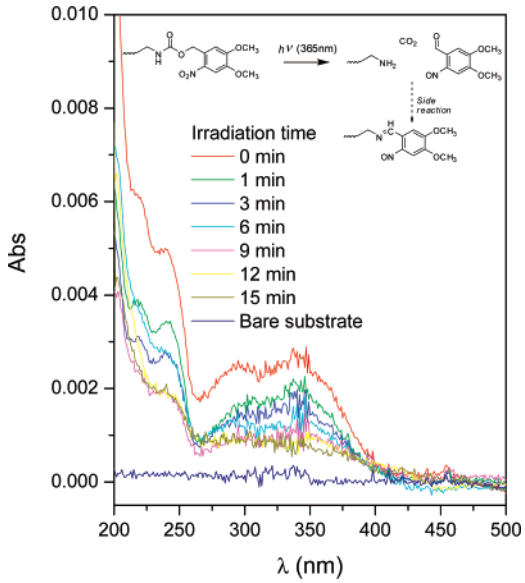

Figure 2. Kinetics of the photolytic reaction of silane **6** on the surface followed by UV spectroscopy.

This causes irreversible retention of the product in the chromatographic column. Better results were achieved by using silica gel that was previously passivated with hexamethyldisilazane (HMDS). This reagent converts the reactive free hydroxylic groups at the surface of the silica gel into inert $Si(Me)_3$. The passivation slightly modifies the polarity of the chromatographic support and, consequently, the final separation process. In general, shorter elution times were detected. Parallel experiments using thin-layer chromatography plates after similar treatment with HMDS helped in assessing the adequate solvent mixture for the separation.

Properties of the Surface Layers. Monocomponent layers of **6** and **8** were obtained by silanization in solution. Anchoring of the molecule to the silica surface occurs through the triethoxysilyl functionality. Trivalent alkoxysilanes favor the formation of denser surface layers than di- or monovalent alkoxysilanes. However, multivalency complicates the surface reaction scenario, since the highly reactive silanol species may condensate not only with the free OH groups of the silica surface but also with each other, forming oligomers. These may lead to larger 3D aggregates and consequently an increase in substantial surface roughness. The progression of these reactions and consequently the characteristics of the final surface layer critically depend on experimental variables such as type of solvent, temperature, and reaction time as well as on the catalyst and the concentration of the organosilane.[33−37] All these parameters were optimized in our case to obtain a dense but smooth surface layer. For this purpose, the course and extent of the surface modification reaction was followed by ellipsometry and UV−vis spectroscopy. The silanization conditions were first varied to maximize the layer thickness and UV−vis absorbance. Substrates obtained in optimized conditions revealed the formation of layers with thicknesses of 2.65 and 1.05 nm and static water contact angles of 57° and 51° for monocompoment layers of silanes **6** and **8**, respectively. (Table 1). The layer thickness is smaller than the molecular length (3.2 and 2.45 nm, respectively) and corresponds to the formation of submonolayers. Assuming a refractive index of 1.4571 for the silane layer, the layer density can be estimated[38,39] (a typical density ρ of 1.0 g cm^{-3} is assumed for an organic layer with a refractive index n of 1.43 and an increment $dn/d\rho$ of 0.24 g cm^{-3}). From the values of the density and the experimental layer thickness, the molar surface loading and surface coverage

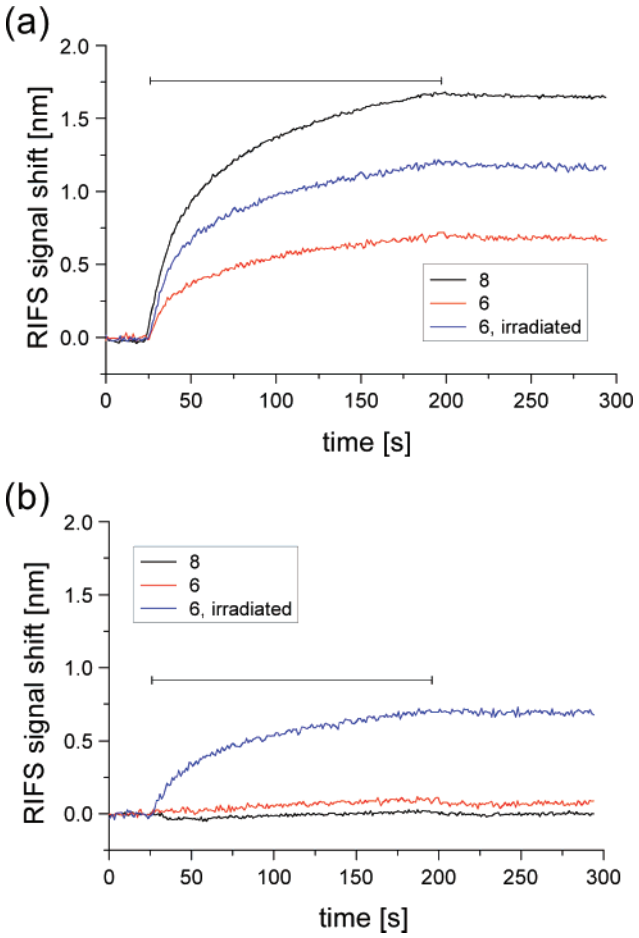

Figure 3. Binding kinetics of streptavidin onto different biotin-functionalized surfaces as followed by RIFS. (a) Biotin coupled to surfaces silanized with either **6** or **8** without additional treatment with acetic anhydride. (b) Biotin coupled to the same surfaces blocked by reaction with acetic anhydride after silanization. The bar marks the injection period of streptavidin. The substrates modified with silane **6** employed for these measurements were not obtained in optimized conditions, and they show reduced silane surface loading and protein binding capacity (see Figure 6 for values corresponding to optimized substrates).

were estimated (Table 1). Surprisingly, a higher surface density was obtained with silane **6**, which is more bulky compared to silane **8** due to the Nvoc protection group. This has been attributed to π-interactions between the terminal Nvoc moieties which promote a more dense packing of this silane.[40,41] Overall, the obtained surface loading values (2.1×10^{12} and 3.2×10^{12} molecules mm^{-2}) are about 1.5−2 times smaller than the typical surface density of a self-assembled monolayer (SAM) of thiols on gold with maximum coverage (4.5×10^{12} molecules mm^{-2}).[42]

Mixed layers were prepared by competitive chemisorption of silanes **6** and **8** from solution using the same experimental conditions as in the case of monocomponent layers to allow meaningful comparison. The amount of water used as catalyst for the silanization turns out to be a crucial parameter, since hydrolyzed **8** is highly insoluble in water or mixtures of water with organic solvents. Modified substrates from feeding solutions with different compositions were prepared (1:1, 1:2, 1:4, 1:9). The amount of photoactive silane **6** on the surface was determined

(41) Halik, M.; Klauk, H.; Zschieschang, U.; Schmid, G.; Dehm, C.; Schütz, M.; Maisch, S.; Effenberger, F.; Brunnbauer, M.; Stellacci, F. *Nature* **2004**, *431*, 963−966.
(42) Love, J. C.; Estroff, L. A.; Kriebel, J. K.; Nuzzo, R. G.; Whitesides, G. M. *Chem. Rev.* **2005**, *105* (4), 1103−1169.

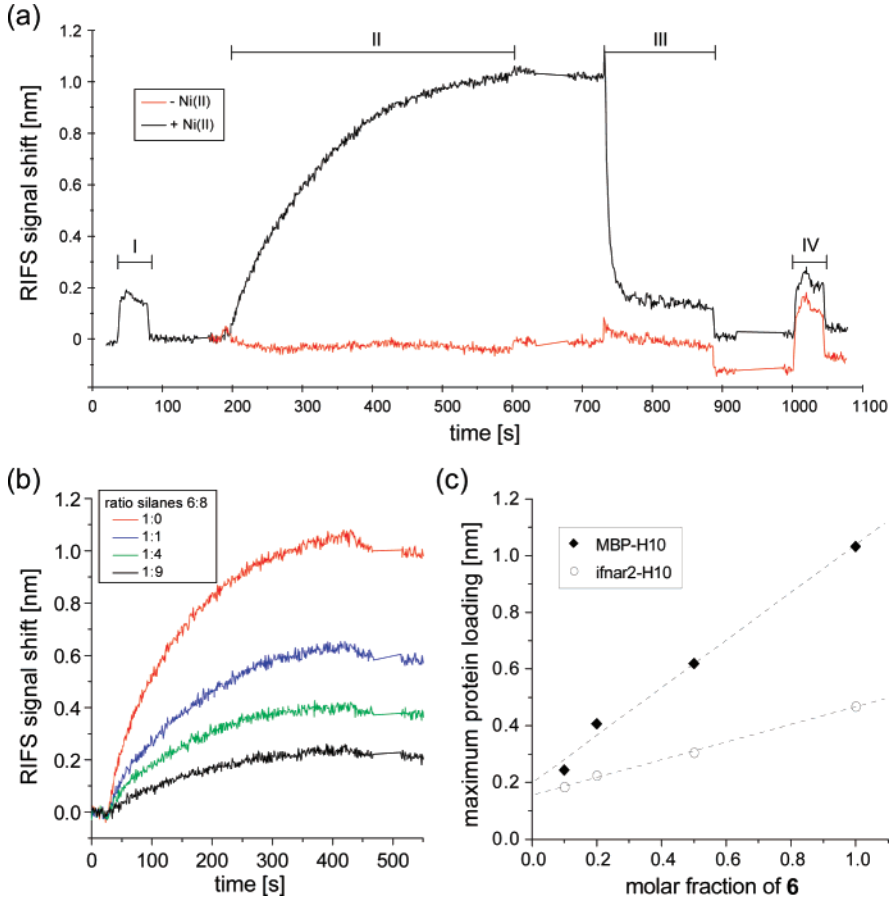

Figure 4. Binding of MBP-H10 to tris-NTA-functionalized surfaces. (a) Typical binding assay on a surface silanized with **6**, followed by blocking with acetic anhydride, deprotection by UV-irradiation, and coupling of tris-NTA (cf. Scheme 1): after loading of the NTA groups with Ni(II) ions (I), 500 nM MBP-H10 was injected (II), followed by elution with 400 mM imidazole (III) and removal of Ni(II) ions by 200 mM EDTA (IV). As a control, the same experiment was performed without Ni(II) loading. (b) MBP-H10 binding to surfaces modified with mixtures of silanes **6**:**8** in different ratios (indicated in the legend) as monitored by RIFS (corrected by the background signals). (c) Binding signals for MBP-H10 and ifnar2-H10 as a function of the molar fraction of silane **6**. The absolute differences in the surface loading observed for MBP-H10 and ifnar2-H10 are due to their different molecular mass (43 kDa for MBP-H10 vs 25 kDa for ifnar2-H10) as well as to the slower binding of ifnar2-H10 due to its highly negative charge.

by measuring the UV absorbance on modified quarz substrates. This analysis revealed a linear correlation between the relative amount of chromophore in solution and on the surface as demonstrated in Figure 1a and b. The contact angle of the modified surface also changes with the ratio of the components: higher contact angles (up to 57°) were obtained with increasing concentration of silane **6** as a consequence of the more hydrophobic character of the Nvoc terminal functionality. A surface layer of silane **8** presents a contact angle of 51°. This value is higher than that obtained from linear grafted PEG layers (CA ∼30°) and also that from star PEG layers (CA ∼45−37°).[43] The layer thickness also increases with increasing concentration of **6**, as expected from its higher molecular length (Figure 1c). This correlation is linear in the mixtures of silanes **6** and **8** up to a monocomponent layer of **6,** but a significant drop in the curve was obtained for the monocomponent layer of silane **8**. These results corroborate that silane **6** reacts more efficiently with the surface than silane **8**, as also reflected by the higher surface loading values when the molar fraction of silane **6** increases (Table 1).

The agreement between solution and surface compositions is not a trivial question in mixed silane layers. Considering that the silanization reaction is complex and highly sensitive to small variations in the reaction conditions (temperature, solvent, water content, and nature of the substrate), the predictability of the final composition of mixed layers is difficult. Another factor to take into account is that each silane, depending on its structure, presents different solubility and hydrolysis/condensation properties which may affect the surface deposition process. In spite of these issues, the optimized experimental conditions seem to yield mixed surface layers which reflect the solution composition.

Regarding the obtained results, and given the fact that it is not possible to quantify silane **8** on the surface, one could think that only silane **6** reacts with the surface. Thus, the decreasing surface concentrations would correspond to the lower solution concentrations of **6** limiting the surface modification reaction. This was ruled out by surface modification experiments with monocomponent solutions of **6** in different concentrations, which always yielded a similar surface density of chromophores, as detected by UV spectroscopy (data not shown).

Photo-deprotection of the Amino Groups. Substrates modified with the photosensitive silane **6** were irradiated at a wavelength of 365 nm (λ_{max}) using a Xe-lamp coupled to a monochromator. Irradiation cleaves the Nvoc group via an intramolecular redox reaction and liberates the reactive amine group at the surface. The photolytic reaction can be followed by the decay of the UV absorbance of the substrate after washing because the chromophore is lost. Figure 2 shows the UV spectra

(43) Groll, J.; Ademovic, Z.; Ameringer, T.; Klee, D.; Moeller, M. *Biomacromolecules* **2005**, *6* (2), 956−962.

of the substrate after different irradiation times. The absorbance dropped 40−50% after 9 min of irradiation, but it did not decrease further with longer irradiation times. This is presumably due to imine formation between the benzaldehyde photofragment and the primary amino group at the surface[12] (scheme in Figure 2). This side reaction reattaches the chromophore to the surface, causing a residual absorbance and decreasing the final density of amine groups. The photolytic reaction also reduces the water contact angle of the surface by 5−8°, indicating the liberation of the more polar amine group. The ellipsometric thickness also decreased after irradiation (Table 1 and Figure 1). The thickness reduction is more noticeable in the substrates with a higher ratio of silane **6**, as expected.

Protein Binding Studies at Functionalized Surfaces. Selective functionalization of the silanized surfaces with biotin and tris-NTA was explored by monitoring protein binding in real time using label-free detection by reflectance interference spectroscopy (RIFS).[44] This technique detects binding on the surface of a thin silica interference layer. Binding curves were obtained from the shift of the interference spectrum. A shift of 1 nm corresponds to 1 ng mm^{-2} protein on the surface. Initially, experiments were performed to analyze the integrity of the surfaces modified with silanes **6** (Nvoc-terminated), **8** (OMe-terminated), and **6** after deprotection (NH_2-terminated) with respect to amine-selective functionalization reactions. For this purpose, these substrates were reacted with biotin *N*-hydroxysuccinimide (NHS) ester and binding of streptavidin was monitored by RIFS (Figure 3a). Fast, stable binding of streptavidin was detected on all substrates, up to saturation values of 1.7 nm (OMe), 1.2 nm (deprotected Nvoc), and 0.6 nm (Nvoc). The binding signal was clearly due to specific interaction with immobilized biotin, because no binding to these surfaces was observed when they were not reacted with biotin NHS ester (data not shown). Surprisingly, substantial binding of streptavidin to Nvoc- and even OMe-terminated layers was observed, which were expected to be inert toward functionalization by the biotin NHS ester. While the reactivity of the Nvoc-protected surface could be explained by undesired hydrolysis of the Nvoc groups during the coupling reaction, this argument does not hold for the OMe-terminated silane. We therefore attributed this reactivity to a possible esterification reaction of free silanol groups by the NHS-active ester, resulting in high amounts of immobilized biotin on all substrates, independently of the presence of amine groups.[45,46] To block all reactive sites capable of reacting with the biotin NHS ester, we incubated all the surfaces in acetic anhydride after silanization. Streptavidin binding experiments with substrates blocked with acetic anhydride prior to irradiation and reaction with biotin NHS ester are shown in Figure 3b. Under these conditions, no streptavidin binding was observed for the OMe-functionalized silane, confirming the specificity of the streptavidin binding. For the non-deprotected Nvoc surface, very little binding of ∼100 pg mm^{-2} was observed, while a significantly higher signal of ∼700 pm was observed for surfaces, which were deprotected prior to the reaction with biotin. Strikingly, a similar difference in streptavidin binding between protected and deprotected Nvoc surfaces (∼600 pm) was observed as for the surfaces which were not blocked with acetic anhydride. Thus, only the background functionalization of the surfaces was minimized by the reaction with acetic anhydride. These results demonstrate that selective functionalization was possible by an improved protocol and that protein binding to these surfaces was highly specific.

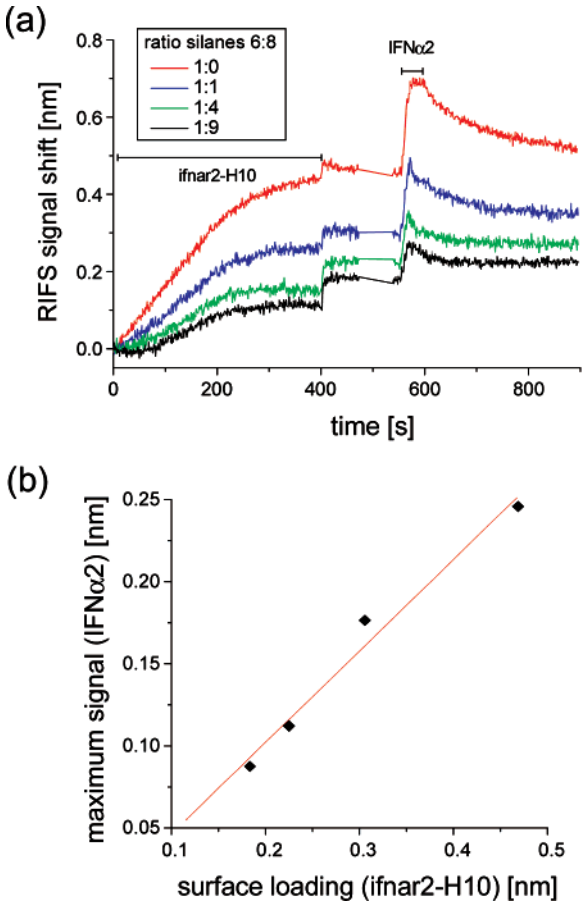

Figure 5. Protein−protein interaction assays on tris-NTA-functionalized surfaces. (a) Immobilization of ifnar2-H10 and binding of its ligand IFNα2 as monitored by RIFS. The surfaces were modified with mixtures of different ratios of silanes **6**:**8** as indicated in the legend, deprotected by UV-irradiation after blocking with acetic anhydride, and then reacted with tris-NTA. (b) Correlation of the binding amplitude observed for IFNα2 with the amount of immobilized ifnar2-H10.

To implement site-specific, reversible immobilization of His-tagged proteins, the multivalent metal chelator tris-NTA was coupled to the amine groups on the surface as shown in Scheme 1b. To optimize the degree of functionalization as well as to minimize nonspecific binding, the silanized substrates were blocked with acetic anhydride prior to UV-irradiation. Maltose binding protein with a C-terminal decahistidine tag (MBP-H10) was immobilized to these surfaces after loading the NTA groups with Ni(II) ions. Results are shown in Figure 4a. Stable immobilization of the protein was observed on all surfaces, which was fully reversible upon injection of imidazole. In the absence of chelated Ni(II) ions, no protein binding was observed, confirming specific capturing through the Ni-tris-NTA/oligo-histidine interaction. The amount of immobilized protein again correlated well with the fraction of Nvoc-functionalized silane on the surface (Figure 4b and c). The MBP-H10 binding signal of 1 nm (i.e., 1 ng mm^{-2}) corresponds to ∼20% of a monolayer (∼5 nm mm^{-2} for a monolayer). Assuming a molecular weight of 43 kDa for MBP-H10, a protein surface concentration of ∼20 fmol mm^{-2} can be estimated.

The functionality of the immobilized protein was probed by capturing the ectodomain of the human type I interferon receptor subunit 2 fused to a C-terminal decahistidine tag (ifnar2-H10), and monitoring the interaction with its ligand IFNα2. The

(44) Piehler, J.; Schreiber, G. *Anal. Biochem.* **2001**, *289* (2), 173−186.
(45) Vikulov, K.; Coluccia, S.; Martra, G. *J. Chem. Soc., Faraday Trans.* **1993**, *89* (7), 1121−1125.
(46) de Lambert, B.; Chaix, C.; Charreyre, M. T.; Laurent, A.; Aigoui, A.; Perrin-Rubens, A.; Pichot, C. *Bioconjugate Chem.* **2005**, *16* (2), 265−274.

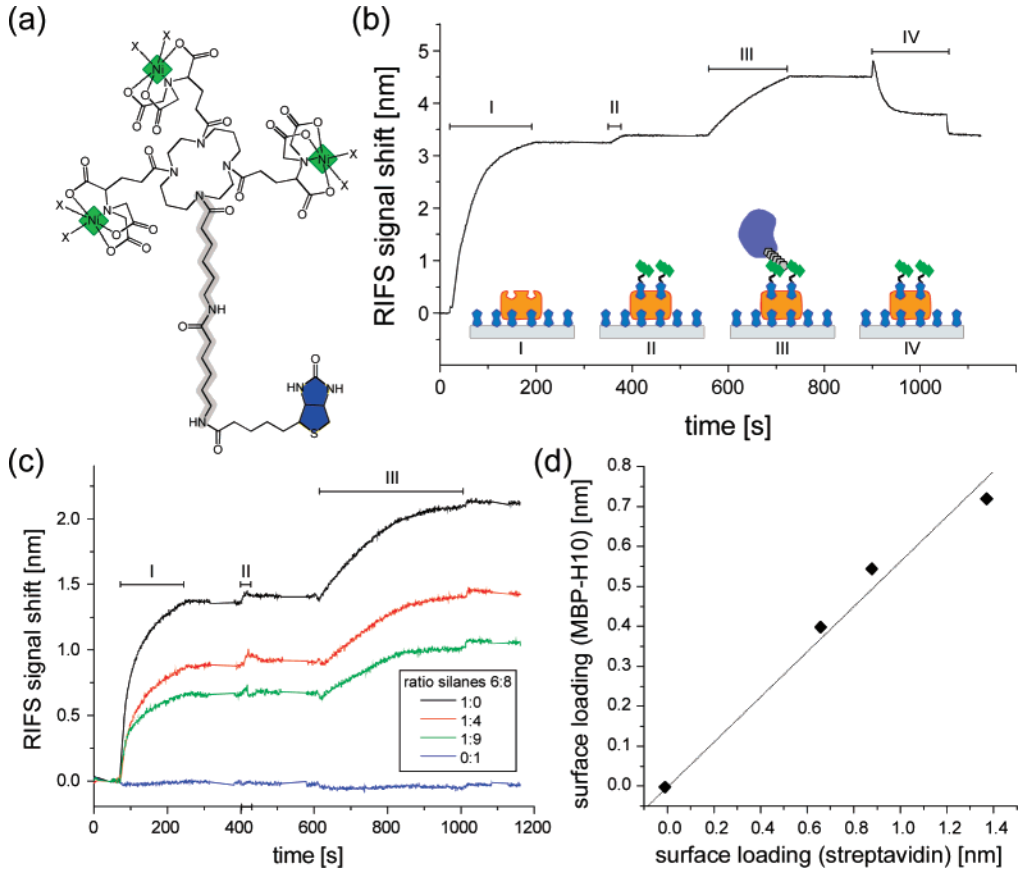

Figure 6. Immobilization of His-tagged proteins on biotin-functionalized surfaces. (a) Structure of tris-NTA biotin. (b) Typical binding assay monitored by RIFS: after binding of streptavidin to the biotin on the surface (I), its remaining biotin binding sites were loaded with ^{BT}tris-NTA (II), followed by injection of MBP-H10 (III). Subsequently, MBP-H10 was removed by injection of imidazole (IV). (c) Binding curves for streptavidin (I), ^{BT}tris-NTA (II), and MBP-H10 (III) to surfaces modified with mixtures of different ratios of silanes **6**:**8** as indicated in the legend. (d) Correlation of the signals of immobilized MBP-H10 with the amount of streptavidin loaded on the surface.

interactions of these proteins has been shown to be highly sensitive to immobilization procedures.[44] Immobilization of ifnar2-H10 followed by binding of IFNα2 as monitored by RIFS is shown in Figure 5. A similar correlation of immobilized ifnar2 with a nominal surface concentration of the Nvoc silane **6** was observed (Figure 4c). Upon injection of the ligand IFNα2, a rapid increase in the signal was observed until saturation binding was reached. Upon rinsing, the ligand dissociated from the surface. The binding kinetics of the interaction was in good agreement with that of previous studies of this interaction.[26,44] Furthermore, excellent correlation of the ligand binding capacity with the amount of immobilized ifnar2 was observed (Figure 5b), confirming the specificity of the interaction. Taking the molecular masses of the proteins into account, about 70% of immobilized ifnar2-H10 was active in terms of ligand binding. Such high activity of this protein on surfaces has only been obtained by specific capturing onto highly biocompatible surfaces.[24,44,47] These results corroborate that the layers obtained by these novel silanes do not only efficiently protect against nonspecific binding but also preserve the folding and functionality of immobilized proteins.

An alternative way for immobilization of His-tagged proteins was implemented with biotin-functionalized surfaces. After binding of streptavidin, a biotin conjugate with tris-NTA (^{BT}-tris-NTA, Figure 6a) was injected, which was rapidly captured by the unoccupied binding sites of streptavidin (Figure 6b). MBP-H10 was stably immobilized on this surface, but it was selectively eluted upon injection of imidazole. No protein binding was observed on surfaces silanized with silane **8** only, confirming the high specificity of functionalization and interaction. The amount of streptavidin bound to surfaces with different compositions correlated well to the amount of MBP-H10 captured through ^{BT}tris-NTA (Figure 6c and d). These results demonstrate the possibility to flexibly implement different immobilization schemes by our approach.

Because of the high affinity of the streptavidin interaction with biotin, quantitative complex formation with the immobilized biotin can be assumed. The streptavidin binding signal of ∼1.4 nm (i.e., ∼1.4 ng mm^{-2}) for monocomponent layers of silane **6** corresponds to ∼30% of a monolayer (∼5 ng mm^{-2} streptavidin). Assuming a molecular weight of 53 kDa for streptavidin, a protein surface concentration of ∼25 fmol mm^{-2} can be estimated. Thus, only ∼1% of the aminosilane molecules on the surface participate in the immobilization under these coupling conditions (assuming that each streptavidin is coupled by 1−2 biotin molecules to the surface.

Functional Patterning. The capability to implement laterally patterned protein immobilization was tested by irradiating the substrates through a mask containing micrometric stripes. This process generates activated areas (those uncaged by irradiation), with the shape of the mask, which were subsequently reacted with different compounds. First, Alexa Fluor 546 succinimidyl ester was coupled to the surface, and the pattern was visualized by fluorescence microscopy. A clear pattern of fluorescent lines on a nonfluorescent background could be observed, and this proved the existence of free amine groups after deprotection (see the Supporting Information). In the second step, site-selective

(47) Tinazli, A.; Tang, J.; Valiokas, R.; Picuric, S.; Lata, S.; Piehler, J.; Liedberg, B.; Tampe, R. *Chem.—Eur. J.* **2005**, *11* (18), 5249−5259.

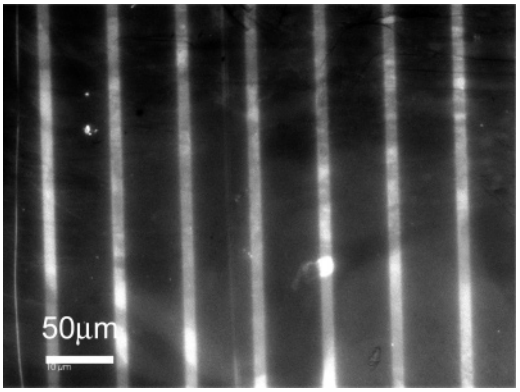

Figure 7. Fluorescence image of patterned substrates after coupling of biotin, followed by incubation of streptavidin and fluorescently labeled biotin.

immobilization of proteins was investigated. For this purpose, biotin NHS ester was coupled to the surface after deprotection through the mask, followed by immobilization of streptavidin. The streptavidin pattern was visualized by fluorescence microscopy after capturing fluorescently labeled biotin to unoccupied biotin binding sites of the immobilized streptavidin (Figure 7). Bright fluorescent stripes with a width of 10 μm were observed, confirming selective binding of fluorescent biotin to the irradiated (active) regions. It is important to note that selectivity is maintained over the three surface coupling steps.

Conclusions

In previous works, we have demonstrated that photocleavable, caged silanes can be used as surface coupling agents to site-selectively immobilize small molecules and colloidal particles at predefined positions on a surface.[12,13] Immobilization is based on surface groups which get activated in selected regions of the substrate upon masked light irradiation, and can then selectively interact with complementary targets from a surrounding solution. The selectivity of this interaction requires a careful design of the surface agent to avoid nonspecific interactions with the caged regions, which would diminish the selectivity of the assembly. Here, we have extended this principle to the site-selective and functional immobilization of proteins. Protein folds are maintained by intramolecular noncovalent interactions, which are perturbed by interaction with the surface, leading to denaturation of immobilized proteins and loss of their function. Consequently, surface layers for protein site-selective immobilization need to contain not only functional groups to enable site-specific attachment, but also molecular elements that prevent nonspecific interactions and thus maintain protein function in the immobilized state. By introducing a TEG unit in the molecular structure of our coupling agent, we have obtained photosensitive surface layers with negligible nonspecific protein adsorption in their caged state, and this enables high levels of specific protein immobilization after functionalization. These results are remarkable considering the shortness of the TEG unit and the fact that we do not have compact SAMs. Upon functionalization of the deprotected amines, specific immobilization of proteins was demonstrated. The amount of immobilized protein or bound ligand was tuned by diluting the surface functionality via coadsorbtion of a reactive and a nonreactive silane. The low nonspecific protein interaction with the surface not only increases the specificity of immobilization and detection but also enables functional protein immobilization. Here, we have demonstrated that a representative protein, the ectodomain of ifnar2, site-specifically immobilized through a His tag remained highly functional in terms of ligand binding. Lateral micropatterning of these surfaces by photodeprotection through a mask provides a flexible means for implementing biofunctionally patterned surfaces. In combination with His-tag-selective, reversible protein capturing by tris-NTA groups demonstrated in this paper, a broad application of this approach for lateral micropatterning of proteins on glass-type surfaces can be envisaged.

Acknowledgment. The authors thank S. Jungbauer for helping with the fluorescence microscope, U. Pawelzik for helping with the synthesis of the compounds, and Gerhard Spatz-Kümbel for support in the synthesis of tris-NTA derivatives. This work was supported by the BMBF (Grant No. 0312034) to J.P. and A.d.C. and by the DFG (Grant No. PI 405/2) to J.P.

Supporting Information Available: Fluorescence image of a substrate modified with silane **6** after masked irradiation and fluorescent labeling with Alexa Fluor 546 succinimidyl ester. This material is available free of charge via the Internet at http://pubs.acs.org.

LA702696B